Adaptive Affine Homogenization Method for Visco-hyperelastic Composites with Interfacial Damage

Youngsoo Kim[1,+], Jiyoung Jung[1,+], Sangryun Lee[1], Issam Doghri[2,*], and Seunghwa Ryu[1,*]

Affiliations

[1]Department of Mechanical Engineering, Korea Advanced Institute of Science and Technology (KAIST), 291 Daehak-ro, Yuseong-gu, Daejeon 34141, Republic of Korea

[2]iMMC, Université catholique de Louvain (UCL), Bâtiment Euler, 4 Avenue G., Lemaître, B1348 Louvain-la-Neuve, Belgium

[+]These authors contributed equally to this work

[*]Corresponding authors e-mail: issam.doghri@uclouvain.be, ryush@kaist.ac.kr

Keywords

Homogenization, Adaptive affine method, Visco-hyperelastic, Composite

- A novel mean-field homogenization method with interfacial damage is proposed

- Effective mechanical behavior of composite consisting of visco-hyperelastic matrix and elastic inclusion is precisely predicted on the time domain.

- Interfacial damage is depicted as an interfacial spring and successfully implemented using an effective inclusion method.

- This method is verified under various loading conditions and strain rates.

Abstract

Despite intense research on the homogenization methods, it still is a challenging task to predict the nonlinear mechanical responses of visco-hyperelastic particulate-reinforced composites. In this work, we propose the adaptive affine method, a novel mean-field homogenization method designed to ensure the consistency of the accumulated strain state and the concentration tensor, and apply the method to predict the mechanical response of the composite in the large strain regime under uniaxial, cyclic, and bi-axial loadings. Our method is also extended to predict the mechanical response in the presence of interfacial imperfections described by linear cohesive traction-separation laws. The analytic predictions are validated against finite element analyses of representative volume elements. We believe that our adaptive affine method can be extended to model various nonlinear responses of load-bearing composites including the effects of (visco)plasticity and finite deformation.

1. Introduction

Particle reinforced composites have been widely adopted to enhance various physical properties including the structural, thermal, thermoelectric, piezoelectric properties, as well as to gain multi-functionality [1-4]. For the industrial development of composites, it is a prerequisite to predict their properties in terms of the composition of their constituents and applied external mechanical, thermal, and electrical stimuli. In that regard, the homogenization theory is well established for the prediction of effective physical properties of composites under a linear response regime. However, there is still room for improvement when it comes to the nonlinear response originated from geometric or material nonlinearity. One typical example of particle reinforced composite in which both geometric and material nonlinearities play a critical role is elastomeric matrix composites. For example, solid propellant materials, which consist of rubbery matrix and oxidizer particles such as aluminum or ammonium perchlorate, have been extensively studied due to their importance in designing high precision rocket and missile propulsion systems [5-10]. Besides solid propellants, visco-hyperelastic elastomer composites are widely used in stretchable electronics, soft robotics, wearable systems, automobile industries, etc. Accordingly, a variety of homogenization frameworks that can appropriately account for such nonlinear responses have been suggested.

Many previous researchers have adopted mean-field homogenization (MFH) approaches to predict the effective properties of solid propellants [11-16]. For the linear elastic response, one can apply the well-established MFH approaches such as the Mori-Tanaka (M-T) scheme which provides a closed-form solution for the effective elastic properties of the composites by utilizing Eshelby's solution for the single inclusion problem. However, for the prediction of inelastic behaviors, multiple methods were suggested to apply MFH and it remains controversial which frameworks provide numerically efficient and mathematically rigorous predictions. A frequency-domain homogenization method was established for linear viscoelastic composites in which the correspondence principle holds by utilizing the Laplace-Carson transform (LCT) [17]. However, the reconstruction of the solution in the time domain involves a costly numerical inversion of the LCT. A similar procedure is followed for the MFH of elasto-viscoplastic composites with an integral affine formulation [18]. Besides being costly, the numerical inversion of the LCT by a collocation method might be inaccurate. Possible improvements have been studied by Rekik and Brenner [19].

On the other hand, significant efforts have been devoted to developing time-domain homogenization methods for the sake of mathematical simplicity and convenience. The linear comparison composite (LCC) concept was proposed to extend linear MFH theories to nonlinear constituents by approaching the actual response within a given time step via virtual linear materials. The LCC can be defined based on variational formulations [20, 21] or the linearization of the local constitutive models. Depending on the linearization scheme, secant or tangent operators are adopted [22-24]. The incrementally affine method was developed using the analogy between linearized elasto-viscoplasticity and thermoelasticity [25] and between linearized viscoelasticity-viscoplasticity and thermoelasticity [26]. However, the incrementally affine method tends to show stiff predictions in the viscoelastic regime. The prediction becomes stiffer in visco-hyperelastic material under finite deformation.

Alternatively, the incremental secant method was developed which combines the advantages of secant modulus and tangent modulus methods [27-30]. The method showed acceptable predictability for materials with elasto-plasticity or elasto-viscoplasticity, but its extension to viscoelastic-viscoplastic composites has not been proposed yet.

In this work, we propose a new homogenization scheme, named the adaptive affine method, that can resolve the aforementioned problems. We found that existing methods suffer from the inconsistency of stress state at t_n when performing the homogenization of linearized material in a given time step $[t_n,\ t_{n+1}]$, i.e. the stress concentration tensor does not correctly indicate the relationship between the applied stress and the stress at the interior of reinforcements. To resolve the problem, we propose a method which adaptively adjusts the strain of each constituent at every step of the loading process to ensure the consistency of the accumulated strain state and the concentration tensor. We utilize the 4th order tangent operator as it is, which enables us to analyze general loading cases including cyclic loading and multi-axial loading under finite deformation. Our method is then extended to predict the mechanical response in the presence of the interfacial imperfections described by a linear cohesive traction-separation law. For the linear interfacial damage model, the interfacial damage is represented as finite compliance of interfacial spring, and the homogenization scheme is implemented using an effective inclusion method. Our homogenization model shows a good match with three-dimensional (3D) finite element model (FEM) simulations.

This paper consists of the following sections. The modeling of visco-hyperelastic material is reviewed based on Simo's model in Section 2. The adaptive affine method is introduced and compared with the incrementally affine method in Section 3. The adaptive affine method for interfacial damage cases is introduced in Section 4. The conclusion is reached in Section 5.

Boldface letters indicate second- or fourth-order tensors and non-bold face letters indicate scalar values. (:) refers to double contraction and ($\otimes$) refers to the dyadic product.

$$\boldsymbol{a}:\boldsymbol{b} = a_{ij}b_{ji};\ \ (\boldsymbol{A}:\boldsymbol{b})_{ij} = A_{ijkl}b_{lk}\ \ (\boldsymbol{a}\otimes\boldsymbol{b})_{ijkl} = a_{ij}b_{kl}$$

2. Visco-hyperelastic material modeling

In this paper, we adopt Simo's visco-hyperelastic model because of the following advantages [31-33]. First, the volumetric or deviatoric part can be selectively chosen as a source of viscosity because the formulation separates the volumetric and deviatoric parts. Second, the model uses a form of strain energy density for the constitutive equation, which allows most of the existing hyperelastic model to be combined. Third, the model can be extended to reflect thermal effects by using the time-temperature superposition principle.

Elastic stress is derived from strain energy density (ψ°) which is additively decomposed into volumetric part (U°) and deviatoric part ($\bar{W}^\circ$) as follows,

$$\psi^\circ = U^\circ(J) + \bar{W}^\circ(\bar{\boldsymbol{C}}) \tag{1}$$

Then, the second Piola-Kirchhoff stress ($\boldsymbol{S}(t)$) is derived from strain energy density with a viscous response as follows,

$$\boldsymbol{S}(t) = JP\boldsymbol{C}^{-1} + \boldsymbol{H} \tag{2}$$

$$\text{where } P = \int_{-\infty}^{t} \frac{K(t-s)}{K_0}\frac{\partial}{\partial s}\left(\frac{\partial U^\circ}{\partial J}\right)ds, \tag{3}$$

$$\boldsymbol{H} = \int_{-\infty}^{t} \frac{\mu(t-s)}{\mu_0}\frac{\partial \bar{\boldsymbol{S}}^\circ}{\partial s}ds, \tag{4}$$

$$\bar{\boldsymbol{S}}^\circ = J^{-\frac{2}{3}}\tilde{\boldsymbol{S}}^\circ = J^{-\frac{2}{3}}\mathrm{DEV}(2\partial_{\bar{c}}\bar{W}^\circ) \tag{5}$$

Here, K and μ are bulk and shear moduli, respectively, J is the determinant of deformation gradient ($\boldsymbol{F}$), and $\boldsymbol{C}$ is the right Cauchy-Green strain tensor ($\boldsymbol{C}$) which is defined as $\boldsymbol{C} \equiv \boldsymbol{F}^T\boldsymbol{F}$. Deviatoric parts of the deformation gradient ($\overline{\boldsymbol{F}}$) and right Cauchy-Green strain tensor ($\overline{\boldsymbol{C}}$) are expressed as $\overline{\boldsymbol{F}} = J^{-1/3}\boldsymbol{F}$ and $\overline{\boldsymbol{C}} \equiv J^{-2/3}\boldsymbol{C}$, respectively. $\partial_{\bar{c}}$ refers to partial derivative with respect to $\overline{\boldsymbol{C}}$. $\mathrm{DEV}(\cdot)$ refers to deviatoric projection operator in the material description which is defined as follows,

$$\mathrm{DEV}(\cdot) = (\cdot) - \frac{1}{3}[(\cdot):\boldsymbol{C}]\boldsymbol{C}^{-1} \tag{6}$$

Viscoelastic properties are represented with the Prony series as follows,

$$\mu(t) = \mu_\infty + \sum_{i=1}^{I} \mu_i \exp(-t/\tau_i) \tag{7}$$

$$\text{where } \mu_0 = \mu(0),\ g(t) \equiv \frac{\mu(t)}{\mu_0},\ g_\infty \equiv \frac{\mu_\infty}{\mu_0},\ g_i \equiv \frac{\mu_i}{\mu_0}$$

$$K(t) = K_\infty + \sum_{j=1}^{J} K_j \exp\left(-t/\eta_j\right) \tag{8}$$

$$\text{where } K_0 = K(0)$$

In this paper, we take only the deviatoric part as a source of viscosity for simplicity, which implies that every K_j is taken to be zero. The elastic tangent operator ($\boldsymbol{L}^\circ$) is expressed as follows,

$$\boldsymbol{L}^\circ = \bar{\boldsymbol{L}}^\circ + 4\left(\frac{\partial^2 U^\circ}{\partial J^2}\frac{\partial J}{\partial \boldsymbol{C}} \otimes \frac{\partial J}{\partial \boldsymbol{C}} + \frac{\partial U^\circ}{\partial J}\frac{\partial^2 J}{\partial \boldsymbol{C}\partial \boldsymbol{C}}\right) \tag{9}$$

$$\bar{\boldsymbol{L}}^\circ = \overline{\boldsymbol{L}_d^\circ} - \frac{2}{3}\left(\overline{\boldsymbol{S}}^\circ \otimes \boldsymbol{C}^{-1} + \boldsymbol{C}^{-1} \otimes \overline{\boldsymbol{S}}^\circ + J^{-2/3}(2\partial_{\bar{c}}\overline{W}^\circ:\boldsymbol{C})\left(\boldsymbol{I}_{\boldsymbol{C}^{-1}} + \frac{1}{3}\boldsymbol{C}^{-1} \otimes \boldsymbol{C}^{-1}\right)\right) \tag{10}$$

$$\begin{aligned}\overline{\boldsymbol{L}_d^\circ} = 4J^{-4/3}\Big[&\partial^2_{\bar{c}\bar{c}}\overline{W}^\circ + \frac{1}{9}(\boldsymbol{C}:\partial^2_{\bar{c}\bar{c}}\overline{W}^\circ:\boldsymbol{C})\boldsymbol{C}^{-1} \otimes \boldsymbol{C}^{-1} - \frac{1}{3}\boldsymbol{C}^{-1} \otimes (\partial^2_{\bar{c}\bar{c}}\overline{W}^\circ:\boldsymbol{C}) \\ &- \frac{1}{3}(\partial^2_{\bar{c}\bar{c}}\overline{W}^\circ:\boldsymbol{C}) \otimes \boldsymbol{C}^{-1}\Big]\end{aligned} \tag{11}$$

$$\text{where } \boldsymbol{I}_{\boldsymbol{C}^{-1}} \equiv \frac{\partial(\boldsymbol{C}^{-1})_{IJ}}{\partial \boldsymbol{C}_{KL}} = -\frac{1}{2}\left[(\boldsymbol{C}^{-1})_{IK}(\boldsymbol{C}^{-1})_{JL} + (\boldsymbol{C}^{-1})_{IL}(\boldsymbol{C}^{-1})_{JK}\right] \tag{12}$$

The elastic tangent operator also can be considered as an instantaneous operator. The first term in Eq. (9) corresponds to the deviatoric part while the second term corresponds to the volumetric part. In the case of Neo-Hookean solids, $\overline{\boldsymbol{L}_d^{\circ}}$ goes to zero. Numerical calculation of the stress including the viscoelastic effect can be obtained as below. Substituting Eq. (7) into Eq. (4), second Piola-Kirchhoff stress at t_{n+1} is expressed as follows,

$$\boldsymbol{S}_{n+1} = J_{n+1}\frac{\partial U^{\circ}(J_{n+1})}{\partial J}\boldsymbol{C}_{n+1}^{-1} + g_{\infty}\overline{\boldsymbol{S}}_{n+1}^{\circ} + \sum_{i=1}^{N} g_i J_{n+1}^{-\frac{2}{3}}\mathrm{DEV}_{n+1}(\boldsymbol{H}_{n+1}^{i}) \tag{13}$$

$\boldsymbol{H}_{n+1}^{i}$ is called an internal algorithmic variable which has an integral form. The detailed process to calculate $\boldsymbol{H}^{i}$ is shown below.

$$\boldsymbol{H}^{i}(t) \equiv \int_{-\infty}^{t} \exp[-(t-s)/\tau_i]\frac{d\tilde{\boldsymbol{S}}^{\circ}}{ds}ds \tag{14}$$

$$\boldsymbol{H}_{n+1}^{i} = \exp(-\Delta t/\tau_i)\,\boldsymbol{H}^{i}(t_n) + \int_{t_n}^{t_{n+1}} \exp[-(t_{n+1}-s)/\tau_i]\frac{d\tilde{\boldsymbol{S}}^{\circ}}{ds}ds \tag{15}$$

$$\boldsymbol{H}_{n+1}^{i} = \exp(-\Delta t/\tau_i)\,\boldsymbol{H}_{n}^{i} + \exp(-\Delta t/2\tau_i)\left(\tilde{\boldsymbol{S}}_{n+1}^{\circ} - \tilde{\boldsymbol{S}}_{n}^{\circ}\right) \tag{16}$$

$\widetilde{\boldsymbol{H}}^{i}$ is newly defined from $\boldsymbol{H}^{i}$ to separate variables within the time step $[t_n,\ t_{n+1}]$.

$$\widetilde{\boldsymbol{H}}_{n}^{i} \equiv \exp(-\Delta t/\tau_i)\,\boldsymbol{H}_{n}^{i} - \exp(-\Delta t/2\tau_i)\,\tilde{\boldsymbol{S}}_{n}^{\circ} \tag{17}$$

$$\boldsymbol{H}_{n+1}^{i} \equiv \widetilde{\boldsymbol{H}}_{n}^{i} + \exp(-\Delta t/2\tau_i)\,\tilde{\boldsymbol{S}}_{n+1}^{\circ} \tag{18}$$

Using $\widetilde{\boldsymbol{H}}^{i}$, the algorithmic tangent operator is obtained as follows.

$$\begin{aligned}\boldsymbol{L}_{n+1}^{alg} = {} & 4\left(\frac{\partial^2 U^{\circ}}{\partial J^2}\frac{\partial J}{\partial \boldsymbol{C}}\otimes\frac{\partial J}{\partial \boldsymbol{C}} + \frac{\partial U^{\circ}}{\partial J}\frac{\partial^2 J}{\partial \boldsymbol{C}\partial \boldsymbol{C}}\right) + g(\Delta t/2)\overline{\boldsymbol{L}_{n+1}^{\circ}} \\ & + \sum_{i=1}^{n} -\frac{2}{3}g_i J_{n+1}^{-2/3}\left(\mathrm{DEV}_{n+1}\left(\widetilde{\boldsymbol{H}}_{n}^{i}\right)\otimes\boldsymbol{C}_{n+1}^{-1} + \boldsymbol{C}_{n+1}^{-1}\otimes\mathrm{DEV}_{n+1}\left(\widetilde{\boldsymbol{H}}_{n}^{i}\right)\right. \\ & \left. + \left(\widetilde{\boldsymbol{H}}_{n}^{i}:\boldsymbol{C}_{n+1}\right)\left(\boldsymbol{I}_{\boldsymbol{C}_{n+1}^{-1}} + \frac{1}{3}\boldsymbol{C}_{n+1}^{-1}\otimes\boldsymbol{C}_{n+1}^{-1}\right)\right)\end{aligned} \tag{19}$$

A detailed derivation of the elastic tangent operator and algorithmic tangent operator is presented in the literature [34].

3. Adaptive affine homogenization in the absence of interfacial imperfection

3.1 Adaptive affine homogenization

We propose the adaptive affine homogenization method which is designed to resolve a common drawback of existing methods, the inconsistency of the accumulated strain state and the concentration tensor. Our method utilizes the Euler forward algorithm in order to avoid an iterative process for numerical integrations and to facilitate the convergence to an accurate solution with small time steps. We use the primary procedure of the incrementally affine method [25, 26] as a preliminary homogenization step to consider inelastic stress change. In the process, each phase of the composite is given the same affine deformation to have the same stress. And then, macro deformation is assigned to remove the virtually loaded affine deformation through the conventional homogenization process, which resulted in the strain increments as below,

$$\Delta\boldsymbol{\varepsilon}_1 = \boldsymbol{A}_1^{\varepsilon}\colon\{\Delta\bar{\boldsymbol{\varepsilon}} + c_0\mathfrak{P}\colon(\Delta\boldsymbol{\sigma}_0^r - \Delta\boldsymbol{\sigma}_1^r)\},\ \ \Delta\bar{\boldsymbol{\varepsilon}} = c_0\Delta\boldsymbol{\varepsilon}_0 + c_1\Delta\boldsymbol{\varepsilon}_1 \tag{20}$$

where c_0 and c_1 are volume fraction of the matrix and particle, respectively, $\Delta\bar{\boldsymbol{\varepsilon}}$, $\Delta\boldsymbol{\varepsilon}_0$, and $\Delta\boldsymbol{\varepsilon}_1$ are the strain increments of the composite, matrix, and particle at a given time step, respectively. In the present paper, subscripts 0 and 1 indicate state variables of the matrix and inclusion phase, respectively. Inelastic stress changes, i.e., stress relaxation of both phases due to viscosity, are shown as $\Delta\boldsymbol{\sigma}_0^r$ and $\Delta\boldsymbol{\sigma}_1^r$. $\boldsymbol{A}_1^{\varepsilon}$ and $\boldsymbol{B}_1^{\varepsilon}$ are strain concentration tensors which are defined in the linear elastic regime as follows,

$$\boldsymbol{A}_1^{\varepsilon} = \boldsymbol{B}_1^{\varepsilon}\colon[c_0\boldsymbol{I} + c_1\boldsymbol{B}_1^{\varepsilon}]^{-1} \text{ where } \Delta\boldsymbol{\varepsilon}_1 = \boldsymbol{A}_1^{\varepsilon}\colon\Delta\bar{\boldsymbol{\varepsilon}} \tag{21}$$

$$\boldsymbol{B}_1^{\varepsilon} = [\boldsymbol{I} + \mathfrak{P}\colon(\boldsymbol{L}_1 - \boldsymbol{L}_0)]^{-1} \text{ where } \Delta\boldsymbol{\varepsilon}_1 = \boldsymbol{B}_1^{\varepsilon}\colon\Delta\boldsymbol{\varepsilon}_0 \tag{22}$$

Here, $\boldsymbol{I}$ and $\mathfrak{P}$ are the fourth-order identity tensor and Hill tensor [35]. $\boldsymbol{L}_0$ and $\boldsymbol{L}_1$ are tangent operator of the matrix and particle, respectively. Detailed explanation for the incrementally affine method can be found in previous papers [25, 26].

In addition to the procedure prescribed by the incrementally affine method, the adaptive affine method considers the modulus change in the deformed state. Because the modulus change over applied loading or time occurs in most nonlinear composites, our method

can be expanded to most types of LCC schemes of nonlinear composite homogenization. We note that the modulus change during each incremental deformation step leads to the mismatch between average strains over each phase and the strain concentration tensor. Moreover, such mismatch accumulates with the repeated incremental deformation procedures. Thus, in the adaptive affine method, a fictitious uniform strain ($\Delta\boldsymbol{\varepsilon}^*$) is augmented to each phase of the composite in order to ensure equality, $\Delta\boldsymbol{\varepsilon}_1 = \boldsymbol{B}_1^{\varepsilon}\colon\Delta\boldsymbol{\varepsilon}_0$. After the augmentation of the fictitious uniform strain, the stress states of matrix and inclusions are written as below,

$$\boldsymbol{\sigma}_0^* = \boldsymbol{L}_0\colon\Delta\boldsymbol{\varepsilon}^* + \boldsymbol{\sigma}_0(t_n) \tag{23}$$

$$\boldsymbol{\sigma}_1^* = \boldsymbol{L}_1\colon\Delta\boldsymbol{\varepsilon}^* + \boldsymbol{\sigma}_1(t_n) \tag{24}$$

The fictitious strain is then tuned to impose the consistency of the strain tensor at the deformed state at t_{n+1}, as below,

$$\boldsymbol{L}_1{}^{-1}(t_{n+1})\colon\boldsymbol{\sigma}_1^* = \boldsymbol{B}_1^{\varepsilon}\colon\boldsymbol{L}_0{}^{-1}(t_{n+1})\colon\boldsymbol{\sigma}_0^*. \tag{25}$$

Substituting Eq. (23) and Eq. (24) into Eq. (25), fictitious uniform strain ($\Delta\boldsymbol{\varepsilon}^*$) is expressed as follows,

$$\Delta\boldsymbol{\varepsilon}^* = (\boldsymbol{I} - \boldsymbol{B}_1^{\varepsilon})^{-1}\colon\left[\boldsymbol{B}_1^{\varepsilon}\colon\boldsymbol{L}_0{}^{-1}(t_{n+1})\colon\boldsymbol{\sigma}_0(t_n) - \boldsymbol{L}_1{}^{-1}(t_{n+1})\colon\boldsymbol{\sigma}_1(t_n)\right] \tag{26}$$

Afterwards, as in the incrementally affine method, an identical macro strain is applied to the composite in order to remove the fictitious deformation. Following the procedure visualized in Fig. 1, the incremental strain change of inclusion satisfying the equality after the incremental deformation is expressed as follows,

$$\Delta\boldsymbol{\varepsilon}_1^{n^*} = c_0\boldsymbol{A}_1^{\varepsilon}\colon\left(\boldsymbol{L}_0^{-1}\colon\boldsymbol{\sigma}_0(t_n) - \{\boldsymbol{I} + \mathfrak{P}\colon(\boldsymbol{L}_1 - \boldsymbol{L}_0)\}\colon\boldsymbol{L}_1^{-1}\colon\boldsymbol{\sigma}_1(t_n)\right). \tag{27}$$

$\boldsymbol{L}_0$ and $\boldsymbol{L}_1$ are newly obtained tangent operators within $[t_n, t_{n+1}]$ which are different from the tangent operators within $[t_{n-1}, t_n]$. We note that even though $\boldsymbol{\varepsilon}_0(t_n)$ and $\boldsymbol{\varepsilon}_1(t_n)$ are adjusted by $\Delta\boldsymbol{\varepsilon}_0^{n^*}$ and $\Delta\boldsymbol{\varepsilon}_1^{n^*}$ in the adaptive affine method, the macro strain of the composite does not change during the process and satisfies the following condition,

$$c_0\Delta\boldsymbol{\varepsilon}_0^{n^*} + c_1\Delta\boldsymbol{\varepsilon}_1^{n^*} = 0. \tag{28}$$

3.2 Application to visco-hyperelastic material

In the finite deformation scheme, there are several options of conjugate stress and strain variables and the corresponding tangent operators. As discussed in the literature [36], it is appropriate to use nominal stress rate, deformation gradient rate, and nominal tangent operator because these stress and strain measures automatically satisfy the basic relation between macro measure and volume-weighted average scheme as follows,

$$\dot{\bar{\boldsymbol{F}}} = c_0\dot{\boldsymbol{F}}_0 + c_1\dot{\boldsymbol{F}}_1 \tag{29}$$

$$\dot{\bar{\boldsymbol{P}}}^T = \mathrm{c}_0\dot{\boldsymbol{P}}_0^T + \mathrm{c}_1\dot{\boldsymbol{P}}_1^T \tag{30}$$

$$\text{where } \dot{\boldsymbol{P}}^T = \boldsymbol{D}:\dot{\boldsymbol{F}},$$

Here, $\boldsymbol{P}^T$ refers to the nominal stress, and $\boldsymbol{D}$ refers to the nominal tangent operator. The superposed dot represents the material time derivative. $\overline{(\cdot)}$ refers to volume averaged value. Our adaptive affine method is applied to study the mechanical response of a highly nonlinear visco-hyperelastic material under finite deformation. The nonlinearity of visco-hyperelastic material has two primary origins. First, the tangent modulus changes with the strain as in a typical hyperelastic material. Second, the nonlinear viscoelastic stress relaxation occurs as in a typical viscoelastic material. The choice of a tangent operator is a critical issue to apply the adaptive affine method and the incrementally affine method to the visco-hyperelastic composite. In section 2, the elastic (instantaneous) and algorithmic tangent operators were presented. The difference between elastic and algorithmic tangent operators depends on time. The elastic tangent operator is defined at the time t_n and thus the elastic tangent operator is identical to the instantaneous tangent operator. However, the algorithmic tangent operator is defined within the time-span $[t_n, t_{n+1}]$. Since the stress relaxation occurs with deformation, the algorithmic tangent operator is usually softer than the elastic tangent modulus mainly by the factor of $g(\Delta t/2)$. From this point of view, it is reasonable to use the elastic tangent operator for the adaptive affine method while the algorithmic tangent operator for the incrementally affine method. Thus, in this paper, the following pseudo-code is devised.

1. Calculate elastic tangent operator of the matrix and inclusion at t_n

2. Convert all material tangent operators ($\boldsymbol{L}_0^\circ$ and $\boldsymbol{L}_1^\circ$) to nominal tangent operators ($\boldsymbol{D}_0^\circ$ and $\boldsymbol{D}_1^\circ$) as follows,

$$D_{KiLj}^\circ = S_{KL}\delta_{ij} + F_{iM}F_{jN}L_{KMLN}^\circ. \tag{31}$$

3. Apply adaptive affine method to get adaptive deformation gradients ($\Delta \boldsymbol{F}_0^{n^*}$ and $\Delta \boldsymbol{F}_1^{n^*}$, Here, $\Delta \boldsymbol{\varepsilon}_i^{n^*}$ and $\boldsymbol{\sigma}_i$ in Eqs. (27, 28) are replaced to $\Delta \boldsymbol{F}_i^{n^*}$ and P_i^T, respectively).

4. Calculate algorithmic tangent operators of the matrix and inclusion for time step $[t_n, t_{n+1}]$.

5. Convert algorithmic material tangent operators ($\boldsymbol{L}_0^{alg}$ and $\boldsymbol{L}_1^{alg}$) to algorithmic nominal tangent operators ($\boldsymbol{D}_0^{alg}$ and $\boldsymbol{D}_1^{alg}$)

6. Apply incrementally affine method with macro deformation gradient ($\Delta \overline{\boldsymbol{F}}$).

7. Update deformation gradient increments ($\Delta \boldsymbol{F}_i$) and stress increments of each phase and go to step 1 for the next deformation increment.

3.3 Validation using FEM for perfect interfacial bonding case

Our homogenization model is verified with the FEM calculation results, using a virtual visco-hyperelastic composite material in which finite deformation and viscoelastic relaxation affect its mechanical response significantly. Commercial software ABAQUS and user-defined material (UMAT) are utilized for homogenization and FEM. We choose the Neo-Hookean model and prony series for the visco-hyperelastic matrix as follows,

$$\psi = \frac{K}{2}(J-1)^2 + \frac{G}{2}\left(J^{-\frac{2}{3}}\mathrm{tr}(\boldsymbol{C}) - 3\right). \tag{32}$$

The inclusion also obeys a Neo-Hookean material, but it is much stiffer than the matrix and thus undergoes very small deformation. The material properties are summarized in Table 1. For the viscous response, only the deviatoric part is taken as a source of viscosity. We refer to values for normalized Prony series from a previous paper [17] as shown in Table 2. The face centered cubic (FCC) structure is adopted as the RVE model for FEM due to two reasons. First, the stress-strain curves of different structures are not very different, and stress-strain curves of randomly distribution structure converge to that of FCC structure with the number of inclusions as shown in Fig. 2. Second, the FCC structure is symmetrical reducing computational cost with good accuracy. Uniaxial cyclic loading tests with different strain rates are conducted to compare our homogenization model and FEM results as shown in Fig. 3. Bi-axial cyclic loading tests with different strain rates are conducted in Fig. 4. As shown in Fig. 3 and Fig. 4,

our homogenization model shows quite a good accuracy. Multi-axial loading tests with a given loading profile are conducted for the different volume fraction of inclusions in Fig. 5. The results show that our model can be applied in a general loading case for visco-hyperelastic composite with good accuracy.

4. Adaptive affine homogenization with interfacial damage

4.1 Linear interfacial damage model-Effective inclusion method

When interfacial damage exists between the matrix and inclusion, the overall mechanical response becomes softer than that of a perfect interfacial bonding case. One of the widely adopted interfacial damage models is the interfacial spring model originally suggested by Qu et al [37, 38] in which the interfacial damage is described by a linear spring layer of vanishing thickness [39]. For the sake of mathematical simplicity, the model has been adopted in the mean-field homogenization scheme by either constructing the modified Eshelby tensor [39-41] or considering an effective inclusion incorporating the interfacial spring compliance [42, 43].

In this paper, we extend the effective inclusion method to finite deformation regimes and implement the method in our homogenization process. Schematics of perfect bonding, interfacial spring model, and effective inclusion model are presented in Fig. 6. In contrast to the perfect bonding case, the interfacial spring model has a displacement jump at the interface originated from the imperfect bonding or damage. The displacement jump increases linearly with increasing interfacial traction because the virtual spring with compliance (β) proportionally relates the displacement jump to the interfacial traction. In this scheme, one has to consider several steps to calculate the modified Eshelby tensor and modified strain concentration tensor to implement the damage into the homogenization process. Here, modified Eshelby tensor and modified strain concentration tensor refer to Eshelby tensor and strain concentration tensor in the presence of interfacial damage, respectively. On the other hand, in the effective inclusion method, the displacement jump effect (interfacial damage) is fully considered by lowering the stiffness of the inclusion. After obtaining the damaged inclusion stiffness tensor, the user can regard it as a perfect bonding case. The detailed process to calculate the damaged inclusion stiffness tensor is shown below. The displacement jump is

expressed by the compliance of the interfacial spring as in the interfacial spring model.

$$\Delta u_i = \beta \Delta P_{Ji} N_J \tag{33}$$

where $\Delta \boldsymbol{u}$ and β are the displacement jump and the compliance of the interfacial spring, respectively. $\boldsymbol{N}$ is the normal vector of the interface in the reference configuration. Due to the displacement jump, macro deformation gradient increment ($\Delta \overline{\boldsymbol{F}}$) is expressed as follows,

$$\Delta \overline{\boldsymbol{F}} = c_0 \Delta \boldsymbol{F}_0 + c_1 \Delta \boldsymbol{F}_1 + c_1 \frac{1}{V_1} \int_{\partial V_1} (\Delta \boldsymbol{u} \otimes \boldsymbol{N}) d\boldsymbol{S} \tag{34}$$

$$= c_0 \Delta \boldsymbol{F_0} + c_1 \Delta \boldsymbol{F_1} + c_1 \frac{\beta}{a} \Delta \boldsymbol{P}_1^T \tag{35}$$

$$= c_0 \Delta \boldsymbol{F}_0 + c_1 \left(\boldsymbol{I} + \frac{\beta}{a} \boldsymbol{D}_1 \right) : \boldsymbol{D}_1^{-1} : \Delta \boldsymbol{P}_1 \tag{36}$$

where a represents the radius of the spherical inclusion. Compared to the perfect bonding case, the only difference is the third term in Eq. (34). As a result, the damaged inclusion stiffness tensor ($\boldsymbol{D}_1^d$) can be defined as follows,

$$\boldsymbol{D}_1^d = \boldsymbol{D}_1 : \left(\boldsymbol{I} + \frac{\beta}{a} \boldsymbol{D}_1 \right)^{-1} \tag{37}$$

By replacing all $\boldsymbol{D}_1$ with $\boldsymbol{D}_1^d$ in the original homogenization process (Eq. (20) and Eq. (27)), the linear interfacial damage can be implemented on the homogenization.

4.2 Validation using FEM for interfacial damage case

The same material properties and structure as in Section 3.3 are used for the validation of interfacial damage cases. The interfacial damage is implemented by cohesive elements on the inclusion surface in FEM. Uniaxial tension tests are conducted with different values of β as shown in Fig. 7. Our model shows a good match with FEM results, but errors increase gradually with strain. We suspect that the errors originate from the difference in reference configuration between homogenization and FEM. The virtual interface spring is defined in the initial configuration in our model while it is redefined in every current configuration in FEM.

5. Conclusion

In this study, we proposed the adaptive affine method which resolves a common limitation of existing homogenization methods, the inconsistency between the strain concentration tensor and the accumulated strain states. The homogenization method shows a good match against FEM simulation results of RVEs under uniaxial or bi-axial cyclic loading conditions or even with multi-axial loading conditions with different loading profiles. We extend our model to interfacial damage cases by adopting an effective inclusion method, which also shows a good match against FEM results for different values of linear interfacial compliance. Although this paper mainly focuses on visco-hyperelastic composite, we believe that the key idea of the adaptive affine scheme can be extended to various nonlinear homogenization models based on the LCC scheme where a dramatic change of tangent operators is involved.

Acknowledgments

The authors acknowledge support by the Basic Science Research Program (2019R1A2C4070690) and Creative Materials Discovery Program (2016M3D1A1900038) through the National Research Foundation of Korea (NRF).

References

[1] S. Ryu, S. Lee, J. Jung, J. Lee, Y. Kim, Micromechanics-based homogenization of the effective physical properties of composites with an anisotropic matrix and interfacial imperfections, Frontiers in Materials 6 (2019) 21.

[2] J. Jung, S. Lee, B. Ryu, S. Ryu, Investigation of effective thermoelectric properties of composite with interfacial resistance using micromechanics-based homogenisation, International Journal of Heat and Mass Transfer 144 (2019) 118620.

[3] J. Jung, S.H. Jeong, K. Hjort, S. Ryu, Investigation of thermal conductivity for liquid metal composites using the micromechanics-based mean-field homogenization theory, Soft Matter (2020).

[4] S. Timilsina, K.H. Lee, I.Y. Jang, J.S. Kim, Mechanoluminescent determination of the mode I stress intensity factor in SrAl2O4: Eu2+, Dy3+, Acta materialia 61(19) (2013) 7197-7206.

[5] M.E. Canga, E.B. Becker, Ş. Özüpek, Constitutive modeling of viscoelastic materials with damage–computational aspects, Computer methods in applied mechanics and engineering 190(15-17) (2001) 2207-2226.

[6] K.-S. Yun, J.-B. Park, G.-D. Jung, S.-K. Youn, Viscoelastic constitutive modeling of solid propellant with damage, International Journal of Solids and Structures 80 (2016) 118-127.

[7] J. Xu, X. Chen, H. Wang, J. Zheng, C. Zhou, Thermo-damage-viscoelastic constitutive model of HTPB composite propellant, International Journal of Solids and Structures 51(18) (2014) 3209-3217.

[8] B. Han, Y. Ju, C. Zhou, Simulation of crack propagation in HTPB propellant using cohesive zone model, Engineering Failure Analysis 26 (2012) 304-317.

[9] G.-D. Jung, S.-K. Youn, A nonlinear viscoelastic constitutive model of solidpropellant, International journal of solids and structures 36(25) (1999) 3755-3777.

[10] R. Nevière, An extension of the time–temperature superposition principle to non-linear viscoelastic solids, International journal of solids and structures 43(17) (2006) 5295-5306.

[11] L. Brassart, H.M. Inglis, L. Delannay, I. Doghri, P.H. Geubelle, An extended Mori–Tanaka homogenization scheme for finite strain modeling of debonding in particle-reinforced elastomers, Computational materials science 45(3) (2009) 611-616.

[12] H. Tan, Y. Huang, C. Liu, P.H. Geubelle, The Mori–Tanaka method for composite materials with nonlinear interface debonding, International Journal of Plasticity 21(10) (2005) 1890-1918.

[13] C. Chiew, M.H. Malakooti, A double inclusion model for liquid metal polymer composites, Composites Science and Technology 208 (2021) 108752.

[14] J.-M. Kaiser, M. Stommel, Modified mean-field formulations for the improved simulation of short fiber reinforced thermoplastics, Composites science and technology 99 (2014) 75-81.

[15] O. Pierard, C. Friebel, I. Doghri, Mean-field homogenization of multi-phase thermo-elastic composites: a general framework and its validation, Composites Science and Technology 64(10-11) (2004) 1587-1603.

[16] H. Shin, J. Choi, M. Cho, An efficient multiscale homogenization modeling approach to describe hyperelastic behavior of polymer nanocomposites, Composites Science and Technology 175 (2019) 128-134.
[17] C. Friebel, I. Doghri, V. Legat, General mean-field homogenization schemes for viscoelastic composites containing multiple phases of coated inclusions, International journal of solids and structures 43(9) (2006) 2513-2541.
[18] O. Pierard, I. Doghri, An enhanced affine formulation and the corresponding numerical algorithms for the mean-field homogenization of elasto-viscoplastic composites, International journal of plasticity 22(1) (2006) 131-157.
[19] A. Rekik, R. Brenner, Optimization of the collocation inversion method for the linear viscoelastic homogenization, Mechanics Research Communications 38(4) (2011) 305-308.
[20] L. Brassart, L. Stainier, I. Doghri, L. Delannay, Homogenization of elasto-(visco) plastic composites based on an incremental variational principle, International Journal of Plasticity 36 (2012) 86-112.
[21] L. Brassart, L. Stainier, I. Doghri, L. Delannay, A variational formulation for the incremental homogenization of elasto-plastic composites, Journal of the Mechanics and Physics of Solids 59(12) (2011) 2455-2475.
[22] I. Doghri, M.I. El Ghezal, L. Adam, Finite strain mean-field homogenization of composite materials with hyperelastic-plastic constituents, International Journal of Plasticity 81 (2016) 40-62.
[23] G. Weng, The overall elastoplastic stress-strain relations of dual-phase metals, Journal of the Mechanics and Physics of Solids 38(3) (1990) 419-441.
[24] G. Hu, Composite plasticity based on matrix average second order stress moment, International journal of solids and structures 34(8) (1997) 1007-1015.
[25] I. Doghri, L. Adam, N. Bilger, Mean-field homogenization of elasto-viscoplastic composites based on a general incrementally affine linearization method, International Journal of Plasticity 26(2) (2010) 219-238.
[26] B. Miled, I. Doghri, L. Brassart, L. Delannay, Micromechanical modeling of coupled viscoelastic–viscoplastic composites based on an incrementally affine formulation, International Journal of solids and structures 50(10) (2013) 1755-1769.
[27] L. Wu, L. Noels, L. Adam, I. Doghri, A combined incremental-secant mean-field homogenization scheme with per-phase residual strains for elasto-plastic composites, International Journal of Plasticity 51 (2013) 80-102.
[28] L. Wu, I. Doghri, L. Noels, An incremental-secant mean-field homogenization method with second statistical moments for elasto-plastic composite materials, Philosophical Magazine 95(28-30) (2015) 3348-3384.
[29] L. Wu, L. Adam, I. Doghri, L. Noels, An incremental-secant mean-field homogenization method with second statistical moments for elasto-visco-plastic composite materials, Mechanics of Materials 114 (2017) 180-200.

[30] M.I. El Ghezal, L. Wu, L. Noels, I. Doghri, A finite strain incremental-secant homogenization model for elasto-plastic composites, Computer Methods in Applied Mechanics and Engineering 347 (2019) 754-781.
[31] P. Haupt, A. Lion, On finite linear viscoelasticity of incompressible isotropic materials, Acta Mechanica 159(1-4) (2002) 87-124.
[32] S. Reese, S. Govindjee, A theory of finite viscoelasticity and numerical aspects, International journal of solids and structures 35(26-27) (1998) 3455-3482.
[33] J.C. Simo, On a fully three-dimensional finite-strain viscoelastic damage model: formulation and computational aspects, Computer methods in applied mechanics and engineering 60(2) (1987) 153-173.
[34] J.C. Simo, T.J. Hughes, Computational inelasticity, Springer Science & Business Media2006.
[35] R. Masson, New explicit expressions of the Hill polarization tensor for general anisotropic elastic solids, International Journal of Solids and Structures 45(3-4) (2008) 757-769.
[36] S. Nemat-Nasser, Averaging theorems in finite deformation plasticity, Mechanics of Materials 31(8) (1999) 493-523.
[37] J. Qu, The effect of slightly weakened interfaces on the overall elastic properties of composite materials, Mechanics of Materials 14(4) (1993) 269-281.
[38] J. Qu, Eshelby tensor for an elastic inclusion with slightly weakened interface, (1993).
[39] S. Lee, Y. Kim, J. Lee, S. Ryu, Applicability of the interface spring model for micromechanical analyses with interfacial imperfections to predict the modified exterior Eshelby tensor and effective modulus, Mathematics and Mechanics of Solids 24(9) (2019) 2944-2960.
[40] Y. Othmani, L. Delannay, I. Doghri, Equivalent inclusion solution adapted to particle debonding with a non-linear cohesive law, International journal of solids and structures 48(24) (2011) 3326-3335.
[41] S. Lee, J. Lee, S. Ryu, Modified Eshelby tensor for an anisotropic matrix with interfacial damage, Mathematics and Mechanics of Solids 24(6) (2019) 1749-1762.
[42] K. Yanase, J.W. Ju, Effective elastic moduli of spherical particle reinforced composites containing imperfect interfaces, International Journal of Damage Mechanics 21(1) (2012) 97-127.
[43] S. Yang, S. Yu, J. Ryu, J.-M. Cho, W. Kyoung, D.-S. Han, M. Cho, Nonlinear multiscale modeling approach to characterize elastoplastic behavior of CNT/polymer nanocomposites considering the interphase and interfacial imperfection, International Journal of Plasticity 41 (2013) 124-146.

Tables

Table 1. Initial elastic properties of each phase.

	Inclusion	Matrix
Shear modulus (G_0) [MPa]	292.32	25.5
Bulk modulus (K_0) [MPa]	633.34	60.0

Table 2. Viscoelastic properties of the matrix.

g_∞	g_i	τ_i
0.003967	0.001497	0.032
	0.00596	0.1
	0.033513	0.316
	0.188428	1
	0.595955	3.162
	0.118909	10
	0.029869	31.623
	0.011891	100
	0.007502	316.228
	0.001497	1000
	0.001012	3162.28

Figures and captions

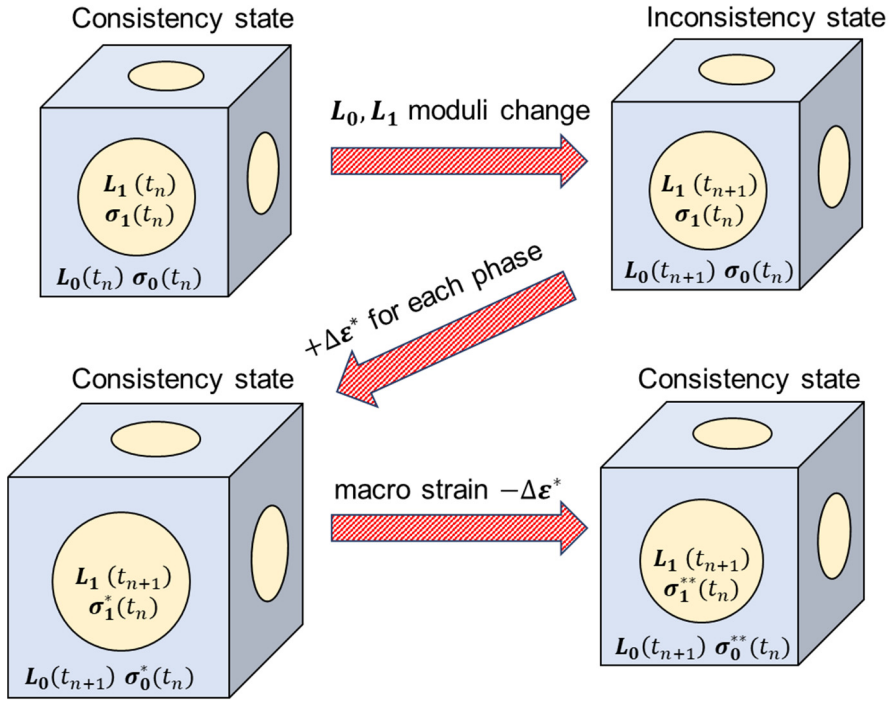

Fig. 1. Schematic of adaptive correction for each strain ($\Delta\boldsymbol{\varepsilon_0^{n^*}}$, $\Delta\boldsymbol{\varepsilon_1^{n^*}}$) satisfying stress concentration between the matrix and particle.

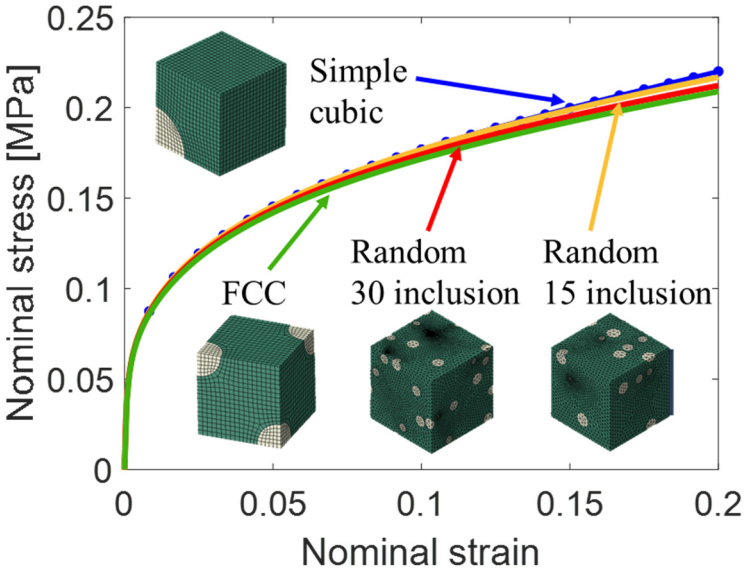

Fig. 2. Biaxial tension tests for visco-hyperelastic composite with different structures. The strain rate is 0.5%/min and the volume fraction of inclusion is 5%.

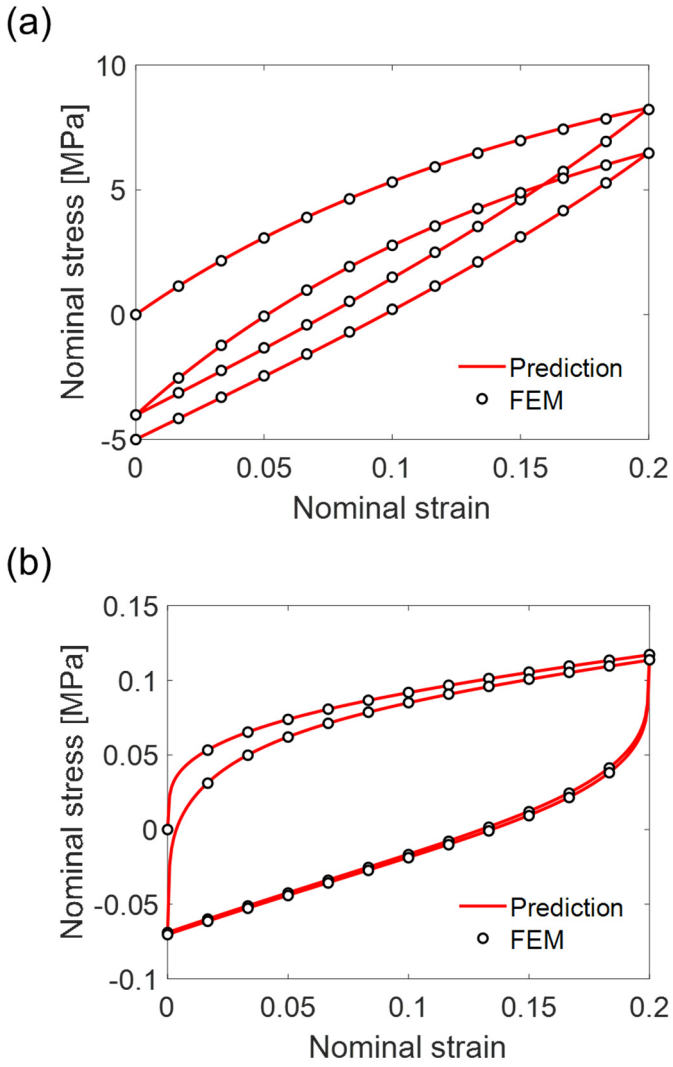

Fig. 3. Uniaxial cyclic loading tests are conducted for visco-hyperelastic composite. Predictions of the homogenization model (lines) are compared with FEM results (symbol). Strain rates are (a) 500%/min and (b) 0.5%/min, respectively. The volume fraction of inclusion is 5%.

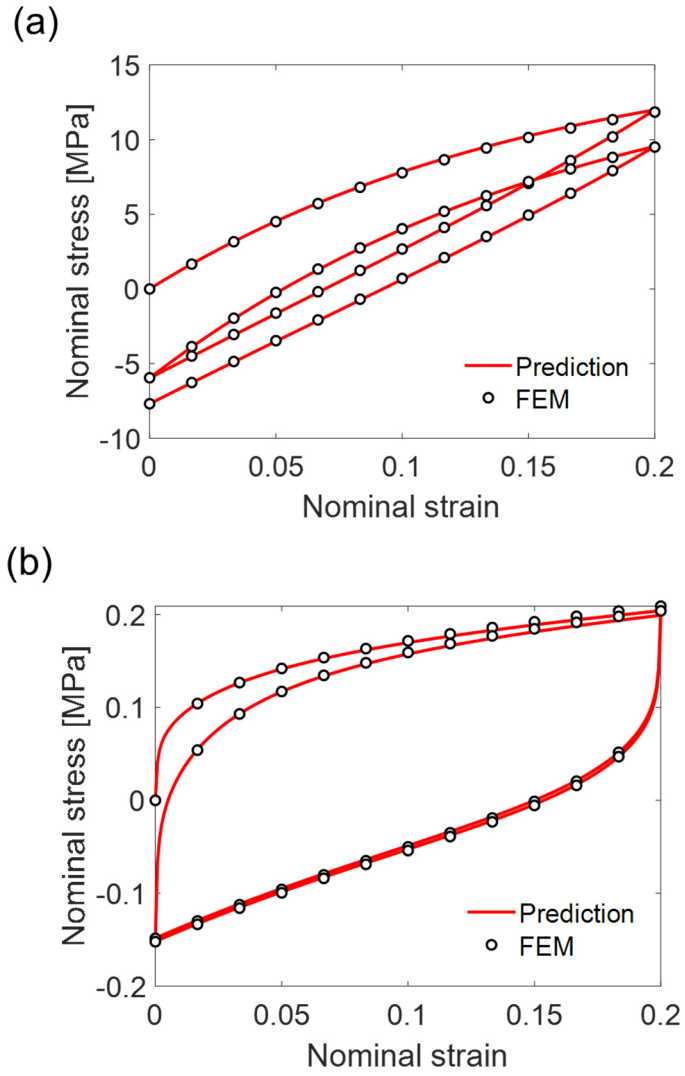

Fig. 4. Bi-axial cyclic loading tests are conducted for visco-hyperelastic composite. Predictions of the homogenization model (lines) are compared with FEM results (symbol). Strain rates are (a) 500%/min and (b) 0.5%/min, respectively. The volume fraction of inclusion is 5%.

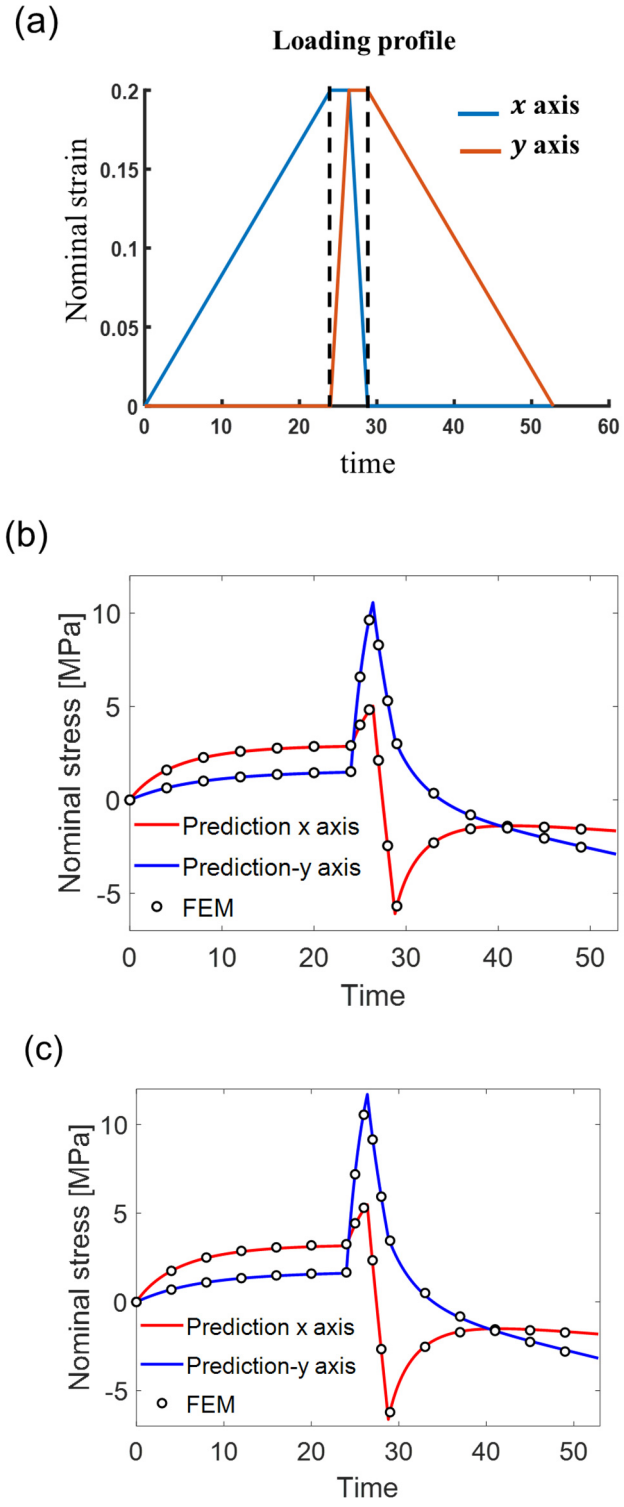

Fig. 5. Multi-axial loading tests are conducted for visco-hyperelastic composite (a) Loading profile is presented. (b, c) Predictions of the homogenization model (lines) are compared with FEM results (symbol). Volume fraction of inclusions are (b) 5% and (c) 10%, respectively.

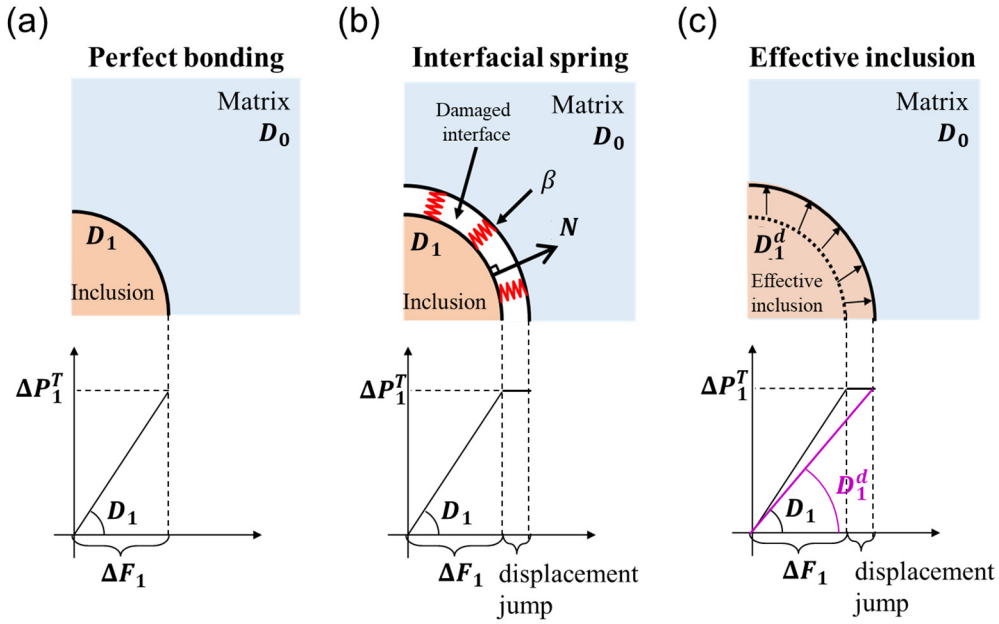

Fig. 6. Schematics of perfect bonding, interfacial spring model, and effective inclusion model.

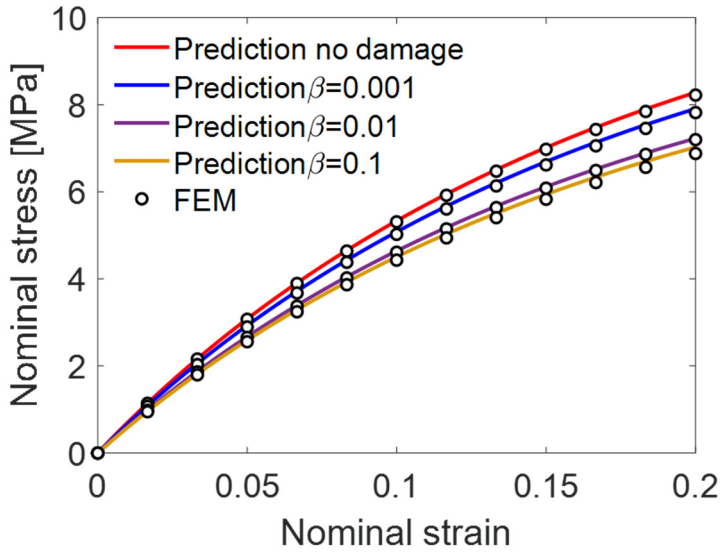

Fig. 7. Uniaxial tension tests with different values of β are conducted. Predictions of the homogenization model (lines) are compared with FEM results (symbol). The strain rate is 500%/min and the volume fraction of inclusion is 5%.